

## Effect of textural properties of Ni (Nano)-supported catalysts on the selective benzene hydrogenation in the vapor phase

Nastaran Parsafard<sup>a,\*</sup>, Mohammad Hasan Peyrovi<sup>b</sup>, Mahdi Abdali Hajiabadi<sup>b</sup>

<sup>a</sup>Department of Applied Chemistry, Kosar University of Bojnord, Bojnord, Iran.

<sup>b</sup>Department of Petroleum Chemistry and Catalysis, Faculty of Chemistry and Petroleum Sciences, University of Shahid Beheshti, Tehran, 1983963113, Iran.

Received 22 September 2018; received in revised form 12 January 2019; accepted 30 April 2019

### ABSTRACT

Ni catalysts supported on Nano porous catalysts were prepared by the impregnation method and tested for vapor phase hydrogenation of benzene. The textural and physico-chemical properties of Ni catalysts were characterized by the X-ray diffraction, Fourier-transform infrared spectroscopy, scanning electron microscope and N<sub>2</sub> adsorption-desorption analysis. The catalytic evaluation revealed that the best selectivity to benzene (> 84%) and high stability with the low coke deposition (< 1.1%) are related to Ni/Folded Sheets Mesoporous Materials-No. 16. The kinetics of benzene hydrogenation has been examined as a function of benzene and hydrogen pressures at various temperatures. Two kinetic models based on power law and Langmuir-Hinshelwood mechanisms were developed for the reaction and compared with the obtained experimental data. The apparent kinetic parameters were estimated using the multiple regression analysis. Both these models present the good results.

**Keywords:** Hydrogenation, Nano porous catalysts, Activity, Stability, Selectivity, Coke deposition.

### 1. Introduction

Environment and human health are seriously damaged by benzene because it is toxic and can cause serious environmental problems [1-4]. On this basis, the petrochemical industry employs the hydrogenation process as one catalytic method for the benzene reduction from engine fuels. The selective hydrogenation of benzene to cyclohexane has importance in both laboratory and industry [5]. Because cyclohexane, unlike benzene, has no toxicity, it is an important chemical material in the production of synthetic nylon intermediates of caprolactam, adipic acid and etc. [5].

The benzene hydrogenation is mostly conducted over less-expensive hydrogenation catalysts, especially nickel-based catalysts. However, because of the thermodynamic limitation of this reaction at high temperatures, it is difficult with those catalysts to achieve a low benzene content [6,7].

The challenge is to develop catalysts with enhanced selective hydrogenation of benzene which this selectivity to benzene among other aromatics is needed for preventing the loss of the octane number of fuels. In this reaction, benzene and hydrogen are adsorbed over the catalysts, where surface benzene undergoes the stepwise additions of hydrogen (Horiuti-Polanyi mechanism) [7-10].

In our previous work, the nature-effect of various supports, such as zeolite, micro-mesoporous composite (HZSM-5-HMS), silicate materials (HMS, SiO<sub>2</sub> and FSM-16), silica-aluminate composite (SiO<sub>2</sub>-Al<sub>2</sub>O<sub>3</sub>), as well as carbonaceous absorbent and composites containing activated carbon and silicate materials (activated carbon-FSM-16), have also been investigated [6, 11-15]. Sun *et al.* have reported 90% conversion for benzene hydrogenation by nickel supported on the carbon nanotube catalyst [16]. Gas phase hydrogenation of the benzene and toluene has been studied by Pushkarev *et al.* The effect of platinum size on the activation energy, turn over frequency, and reactant relative orders, was investigated. The results indicate

\*Corresponding author.

E-mail address: n-parsafard@kub.ac.ir (N. Parsafard)

that the reaction is structure-sensitive [17]. Akbayrak detected the performance of the rhodium catalyst supported over ceria. It became clear that this catalyst showed the better performance than titania, zirconia and hafnia supported Rh Catalysts [18]. Li *et al.* also studied the effect of different morphologies of ceria crystals loaded with palladium in the hydrogenation reaction of benzene. The results confirm that the PC100 catalyst with the conversion of 96% exhibits a very acceptable performance for this reaction in the gas phase [19].

In the last few years, porous materials are widely used in the chemical industry as a support for reduced Ni catalysts. These molecular sieves contain a huge number of pores with different geometry, size and various shapes, high thermal stability and surface area [20,21].

Though various studies about porous-supported catalysts for benzene hydrogenation have been reported [11,20,21], the effect of support pore size is an interesting subject. Therefore, this work aims to shed light on the effect of the pore size diameter of nickel supported mesoporous silica on selective hydrogenation of benzene in the mixture of aromatics. Catalyst activity, product selectivity, catalysts stability and their kinetics were evaluated in a fixed-bed reactor.

## 2. Experimental

### 2.1. Catalyst preparation methods

Hexagonal Mesoporous Silica (HMS) was synthesized by the sol-gel method reported by our group [3]. Surfactant (dodecylamine) was added to the very dilute solution of HCl with stirring for 5 min. When the solution became homogeneous, ethanol and tetraethyl orthosilicate were added with continued stirring, and the obtained gel was aged for 18 h. The resulting product was filtered, washed with distilled water, and then dried at room temperature. The obtained solid was calcined at 600 °C in air for 6 h and designated as HMS.

12.0 g amorphous silica and 8.0 g NaOH were dissolved in 100 mL methanol in preparation of Folded Sheets Mesoporous Materials-No. 16 (FSM-16) [22]. This solution was stirred at room temperature for 3 h. Then it was dried at 100 °C for 2 weeks and calcined at 600 °C for 6 h. 2 g of kanemite was added to 25 ml of cetyltrimethylammonium bromide (CTAB, 0.1 M) and heated at 70 °C for 150 min with stirring (pH=8.5). The obtained solid was filtered, washed, dried and calcined at 600 °C for 6 h.

The described method by Khalil [23] was used to prepare SBA-15 by 4 g of the triblock copolymer Pluronic P123 dissolved in 30 g of water. Then 120 g of 2 M HCl and 8.5 g of TEOS were added to this solution

with stirring at 35 °C for 20 h. The obtained biphasic solution was kept at 80 °C overnight. After pouring out the aqueous phase (upper phase), the concentrated phase (lower phase) was separated and washed several times with deionized water and ethanol. The solid product was air-dried at room temperature for 24 h, followed by calcination at 500 °C for 8 h.

Mobile Crystalline Material-No. 41 (MCM-41) was prepared according to the procedure described in [24]. Typically, 2.4 g CTAB was dissolved and stirred with 120 g of deionized water. After the formation of homogenized solution, 10 mL of ammonium hydroxide was added to it. Then the mixture was stirred for 5 min with adding 10 mL of TEOS. The resultant mixture was heated in an oven at 100 °C for 16 h. The as-synthesized solid was filtered, washed with water repeatedly and then dried at 110 °C overnight, followed by calcination at 500 °C for 8 h.

Moreover, Ni (25 wt%) catalysts were prepared by the wetness impregnation method over the supports with nickel (II) nitrate hexa hydrate (0.2 M) at 70 °C to achieve a gel. After evaporating the solvent and drying in the oven at 100 °C for 12 h, the Ni-supported catalysts were calcined in air at 300 °C for 4 h. It should be noted that all materials were purchased from Merck and Aldrich companies and were used as received without any further purification.

### 2.2. Catalyst characterization

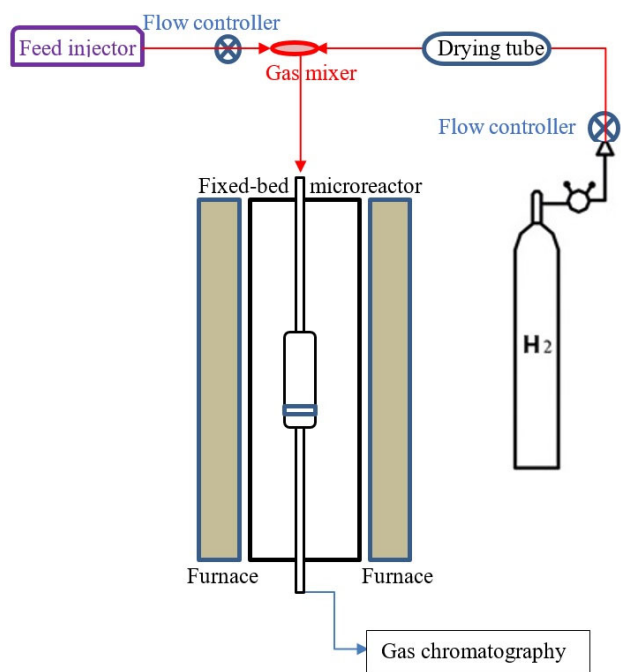
X-ray diffraction (XRD) patterns of the prepared powders, in the 0° to 80° 2θ range, were acquired with an X-PERT diffractometer using Cu K<sub>α</sub> radiation at 45 kV and 50 mA. The average particle size was calculated from the broadening of the main diffraction peak using the Scherrer equation [6]. N<sub>2</sub> BET (Brunauer–Emmet–Teller) isotherms were obtained using an all-glass high-vacuum line on an ASAP-2010 micromeritics gas sorption analyzer. The total pore volumes (V<sub>p</sub>) were estimated according to the nitrogen uptake at a relative pressure (P/P<sub>0</sub>) of ca. 0.99. The mesopore size distributions were derived from the adsorption branch of the N<sub>2</sub> isotherms using the Barrett-Joyner-Halenda (BJH) method. FTIR spectra were recorded on a BOMEM spectrometer model Arid-Zone, where the samples were ground with KBr and pressed into the wafer. Thermo gravimetry (TG) and differential thermal analysis (DTA) were measured with a STA503 M instrument. The samples were heated from room temperature to 800 °C at a heating rate of 10 °C/min under a 5 vol.% O<sub>2</sub>/N<sub>2</sub> flow of 60 ml min<sup>-1</sup>. Field emission scanning electron microscope (SEM, HITACHI S-4160) was employed to observe the morphology of the catalysts.

### 2.3. Catalytic testing

#### 2.3.1. Activity and stability

Benzene hydrogenation experiments were carried out in gas phase at atmospheric pressure in a continuous fixed bed microreactor with a feed hydrogen-to-benzene (Bz)/toluene (Tu)/xylene (Xy) (Merck, >99%) volume ratio of 120:1. The reactor effluent was analyzed by means of an online gas chromatograph (Agilent Technologies 7890A equipped with a flame ionization detector). The fixed bed microreactor is a Pyrex glass reactor (Scheme 1). The reaction temperature was monitored by a thermocouple put in a thermowell at the center of the catalytic bed. The required catalyst loading was about 0.3 g (to avoid the mass transfer limitations). In a typical run, the catalyst was reduced prior to the reaction in the following way. First, it was heated in flowing  $H_2$  ( $40 \text{ ml min}^{-1}$ ) up to  $400 \text{ }^\circ\text{C}$  and it was kept for 2 h at this temperature. Then, the catalyst was cooled to  $130 \text{ }^\circ\text{C}$  while keeping the same  $H_2$  flow rate for 1 h. Afterward, the flow rates of aromatics were set ( $2 \text{ ml h}^{-1}$ ) and the gas mixture was passed over the catalyst. The activity of the catalyst was followed with standard experiments at  $130\text{-}190 \text{ }^\circ\text{C}$  reaction temperatures. Cyclohexane was significantly observed in the product stream.

The major problem with the catalytic performances is their poor stability due to deactivation by carbon deposition. In order to study the catalytic stability during the hydrogenation of benzene, the following experiment was performed: each catalyst was put in contacted with



**Scheme 1.** A schematic diagram of the fixed-bed reactor.

mentioned feed at a selected temperature ( $150 \text{ }^\circ\text{C}$ ) for 72 h. Benzene and the reaction products were analyzed at a certain period of time with gas chromatograph, operated with a flame ionization detector (FID).

#### 2.3.2. Kinetics measurements

The kinetics study was carried out using the mentioned reactant mixture. In this study, the partial pressures of hydrogen and aromatics mixture were changed. The samples were heated from  $130$  to  $190 \text{ }^\circ\text{C}$ . The tests were conducted at each temperature. The rate of heating was  $20 \text{ }^\circ\text{C h}^{-1}$ . The catalyst was cleaned in a hydrogen flow after each test. The reaction products were analyzed by GC in the same conditions as for the hydrogenation of benzene.

## 3. Results and Discussion

### 3.1. Physico-chemical characterization

The XRD patterns of the calcined nanoporous silicate samples are shown in Fig. 1. The siliceous Ni-supported catalysts present a pattern that corresponds to highly hexagonal ordering of the mesopores. Ni/MCM-41 catalyst exhibits the narrow  $d_{100}$  reflection at  $2^\circ$  and the presence of the higher order  $d_{110}$ ,  $d_{200}$  and  $d_{210}$  reflections at about  $4^\circ$ ,  $5^\circ$  and  $6^\circ$ , respectively. Diffractogram of the Ni/SBA-15 shows  $p6mm$  hexagonal arrangement of the mesopores with three reflections indexed to  $d_{100}$ ,  $d_{110}$  and  $d_{200}$  planes. A very strong peak of  $d_{100}$  reflection is also observed in the patterns of Ni/HMS and Ni/FSM-16 catalysts. The diffraction patterns of the catalysts show other peaks, which can be indexed as Ni, NiO and  $Ni(OH)_2$ . These peaks are pointed out in figure [20,25].

Fig. 2 illustrates the FTIR spectra of the mesoporous catalysts after calcination in the wavenumber region of  $4000\text{-}400 \text{ cm}^{-1}$ .

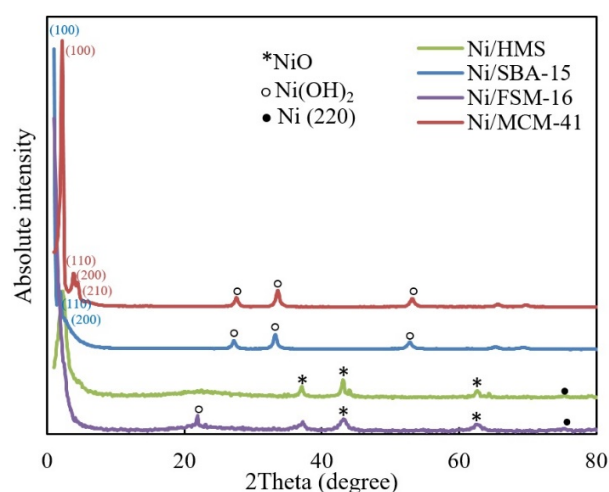


**Fig. 1.** XRD patterns of Ni catalysts supported on SBA-15, MCM-41, HMS and FSM-16.

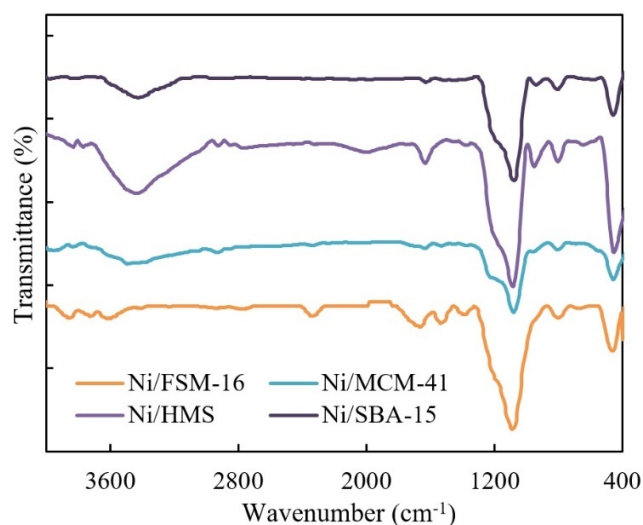


**Fig. 2.** FT-IR spectra of nickel/mesosilicates.

The bands at about  $3500\text{ cm}^{-1}$  and  $1600\text{ cm}^{-1}$  are the bending vibration of the hydroxyl stretch and physisorbed water. The asymmetric and symmetric stretch bands of Si–O–Si are observed at  $1170\text{ cm}^{-1}$  and  $1090\text{ cm}^{-1}$  and  $779\text{ cm}^{-1}$ , respectively. The Si–O bending vibration is detected at  $455\text{ cm}^{-1}$ . The weak band at  $941\text{ cm}^{-1}$  is assigned to the bending vibration of Si–OH group [25].

The catalyst surface area and pore size/volume determined by  $\text{N}_2$  adsorption-desorption analysis, were given in Table 1. As the results show, all calcined samples except Ni/SBA-15, exhibit high surface areas ( $709\text{--}901\text{ m}^2/\text{g}$ ) and mean pore diameters of  $1.6\text{--}3.9\text{ nm}$ . The highest surface area was obtained for the Ni/MCM-41 catalyst.

SEM micrographs of the calcined catalysts (Fig. 3) show the spherical-like structures for mesoporous materials. Furthermore, these images show the structure and aggregated-shape of FSM-16.

### 3.2. Activity results

The selective catalytic performance has been performed on Ni supported mesoporous catalysts. The catalysts

activities were assessed by hydrogenation performance of benzene (Bz) in the presence of toluene (Tu) and xylene (Xy) over prepared catalysts between  $130$  and  $190\text{ }^\circ\text{C}$ . Under our experimental conditions, the most detectable products of the reaction were cyclohexane (CH) and methyl cyclohexane (MCH), respectively. Table 2 reports the results of catalytic activity such as the conversion (Eq. 1), overall conversion (Eq. 2), selectivity to Bz (Eq. 3) and yield to Bz (Eq. 4) in various temperatures.

$$C_{Bz\text{ (or Tu)}} = \text{percentage of Bz (or Tu) transformed into CH (MCH)} \quad (1)$$

$$C_{ov}(\%) = (m_{Bz}C_{Bz} + m_{Tu}C_{Tu} + m_{Xy}C_{Xy}) \times 100 \quad (2)$$

$$S_{Bz}(\%) = \frac{m_{Bz}C_{Bz}}{C_{ov}} \times 100 \quad (3)$$

$$Y_{Bz}(\%) = \frac{C_{Bz} \cdot S_{Bz}}{100} \quad (4)$$

There is a different behavior for the prepared catalysts in the conversion versus temperature. However, in general, it can be said that by increasing the temperature, the conversion increases up to a certain temperature, and then the downward trend can be observed probably because of the different capacities that catalysts have in the adsorption of benzene molecules.

By evaluating the conversion of the prepared catalysts, the Ni/SBA-15 has the best conversion for benzene and xylene, and the Ni/HMS catalyst shows 100% conversion for toluene.

Based on the primary aim of the present work and to eliminate the harmful effects of benzene and to prevent the loss of the octane number of fuel, a catalyst would be desirable for us to have a high conversion for benzene with a minimal change in the amount of toluene and xylene. Therefore, in order to make better decisions about the best catalyst, benzene selectivity and reaction yield were also calculated. The results of these two parameters indicate that the catalyst Ni/FSM-16 has the best performance compared to other catalysts.

**Table 1.** Physical and chemical properties of mesoporous catalysts.

Catalysts	Ni/HMS	Ni/FSM-16	Ni/SBA-15	Ni/MCM-41
$S_{BET}$ ( $\text{m}^2/\text{g}$ ) <sup>a</sup>	763	709	302	901
$V_p$ ( $\text{cm}^3/\text{g}$ ) <sup>b</sup>	0.74	0.52	0.66	0.54
$W_p$ (nm) <sup>c</sup>	3.9	2.7	7.8	1.6
$d_{Ni}$ (%) <sup>d</sup>	22.7	17.0	9.1	32.2

<sup>a</sup>BET surface area.

<sup>b</sup>Average pore volume ( $V_p$ ) by BJH desorption.

<sup>c</sup>Average pore width ( $4V/A$ ) by BET ( $W_p$ ).

<sup>d</sup>Ni dispersion determined by  $\text{H}_2$  chemisorption.

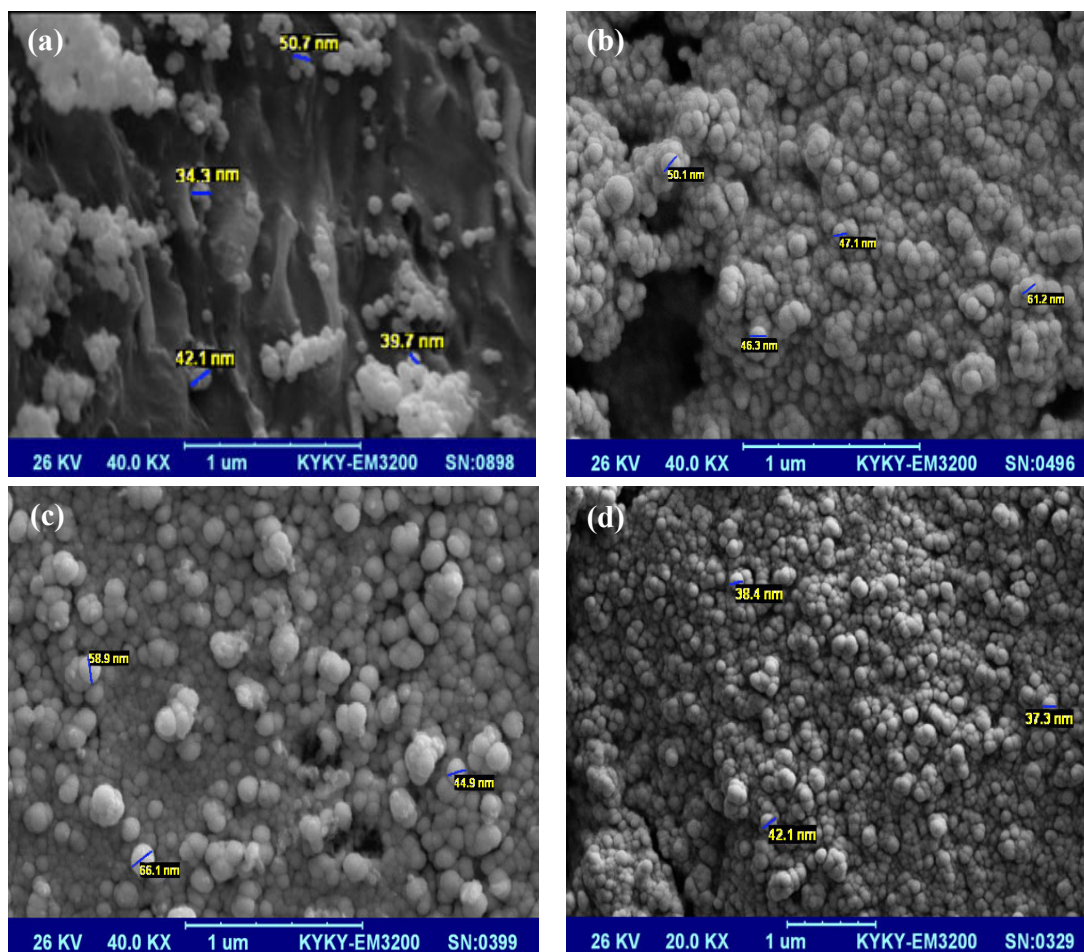


**Fig. 3.** SEM images of (a) Ni/FSM-16, (b) Ni/SBA-15, (c) Ni/MCM-41 and (d) Ni/HMS.

**Table 2.** Temperature effect on catalytic performance.

Catalysts	T (°C)	C <sub>Bz</sub>	C <sub>Tu</sub>	C <sub>Xy</sub>	C <sub>Ov</sub>	S <sub>Bz</sub>	Y <sub>Bz</sub>
Ni/HMS	130	61.6	100.0	0.0	86.2	25.7	15.9
	150	100.0	100.0	0.0	100.0	36.0	36.0
	170	23.5	100.0	0.0	72.5	11.7	2.7
	190	21.4	100.0	0.0	71.7	10.8	2.3
Ni/FSM-16	130	29.1	12.6	0.0	18.5	63.3	18.4
	150	36.4	5.1	0.0	16.4	80.0	29.1
	170	56.5	7.9	0.0	25.4	84.2	47.6
	190	56.0	55.0	0.0	55.3	43.3	24.2
Ni/SBA-15	130	72.7	59.8	85.4	100.0	26.2	19.0
	150	73.5	53.0	80.7	94.1	28.1	20.6
	170	84.4	45.7	80.2	93.2	32.6	27.5
	190	92.4	40.8	89.4	98.0	33.9	31.3
Ni/MCM-41	130	59.4	37.6	28.2	63.4	33.7	20.0
	150	53.8	32.3	0.0	40.0	48.4	26.0
	170	53.3	37.6	0.0	43.2	44.4	23.7
	190	58.4	48.6	5.7	55.8	37.7	22.0

The performance of the catalysts based on these two parameters is as the follows:

Ni/FSM-16 > Ni/MCM-41 > Ni/SBA-15 > Ni/HMS

The Ni/FSM-16 catalyst exhibits the highest selectivity (84.2%) and the reaction yield (47.6%) at 170 °C.

The stability of these mesoporous catalysts against the deposition of carbon was also investigated. The stability test is very crucial because in the reactions that deal with the hydrocarbon feed, the formation of carbon over the period of time can be observed as a loss of activity in the catalysts. On this basis, the stability of Ni-supported catalysts under the hydrogenation process was performed at 150 °C for 72 h. From the obtained results as listed in Table 3, the Ni/SBA-15 catalyst has good stability in hydrogenation of benzene with the lowest carbon deposition (from TGA results) at 150 °C in this period of time. However, Ni/MCM-41 and Ni/FSM-16 are also close to it. According to the N<sub>2</sub> adsorption-

desorption results (Table 1), it seems that the textural properties are the reason for the good performance of Ni/FSM-16 in catalytic hydrogenation of aromatics.

### 3.3. Kinetics test

The orders of reaction with respect to benzene and hydrogen were determined by following the rate of Bz consumption under various combinations of Bz and H<sub>2</sub> partial pressures. Kinetics data were determined over the range of partial pressures of reactants as 2.3-5.2 Pa for benzene and 7.1×10<sup>-5</sup> to 3.1×10<sup>-4</sup> Pa for hydrogen. Table 4 and Fig. 4 show the rate-temperature measurements done in this study. A regression of the rate data at all temperatures in the power-law (PL) model gave the parameter estimates reported in this table. Fig. 4c shows the parity plot of PL model with a correlation coefficient (R<sup>2</sup>) of 1.0. PL model is expressed based on the partial pressures of Bz (P<sub>Bz</sub>) and H<sub>2</sub> (P<sub>H2</sub>).

**Table 3.** The effect of time on stream (TOS) on the activity of catalysts.

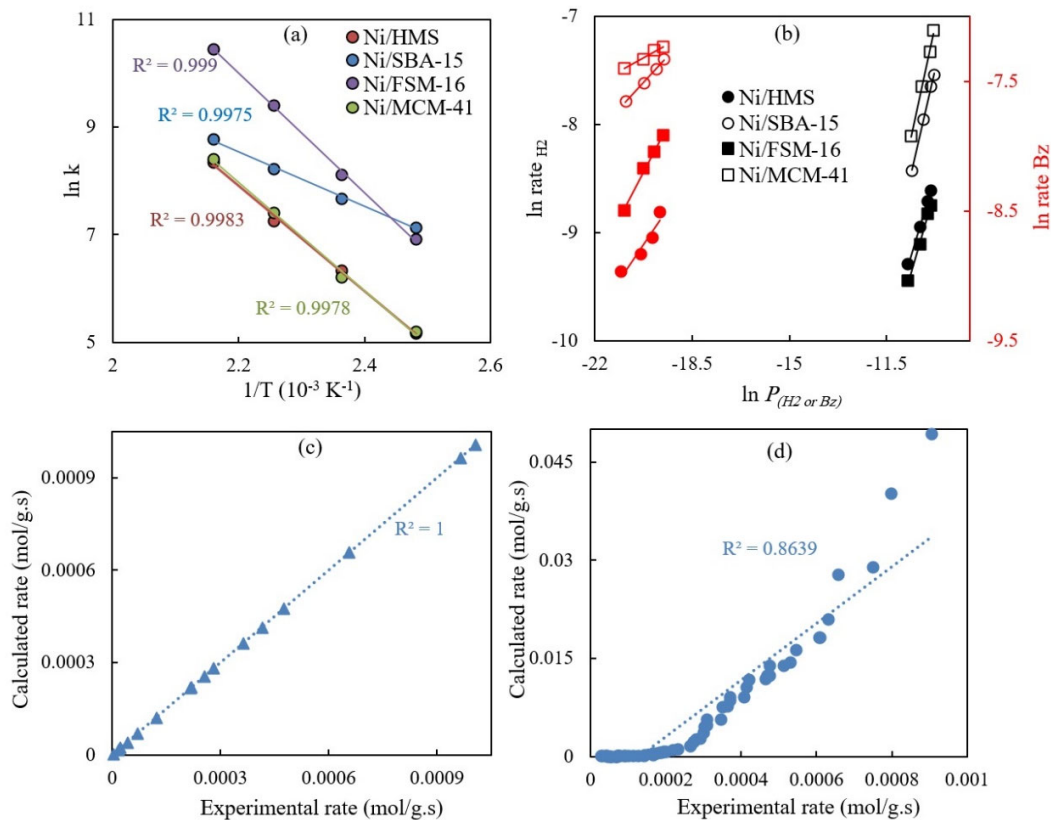
TOS (h)		1	3	5	7	9	12	24	48	72	C (%)
Ni/HMS	C <sub>Bz</sub>	100.0	85.4	78.4	76.7	72.7	70.0	68.0	61.0	57.4	3.4
	C <sub>Tu</sub>	100.0	79.2	66.3	56.6	54.4	47.3	43.0	39.5	30.1	
	C <sub>Xy</sub>	0.0	0.0	0.0	0.0	0.0	0.0	0.0	0.0	0.0	
	C <sub>Ov</sub>	100.0	81.5	70.6	63.8	61.0	55.5	52.0	47.2	39.9	
	S <sub>Bz</sub>	36.0	37.8	40.0	43.3	42.9	45.4	47.1	46.5	51.8	
	Y <sub>Bz</sub>	36.0	32.2	31.3	33.2	31.2	31.8	32.0	28.4	29.7	
Ni/FSM-16	C <sub>Bz</sub>	36.4	30.4	29.2	28.2	24.3	21.4	20.6	18.4	17.8	1.1
	C <sub>Tu</sub>	5.1	4.8	4.4	4.2	2.6	2.3	2.2	1.9	1.6	
	C <sub>Xy</sub>	0.0	0.0	0.0	0.0	0.0	0.0	0.0	0.0	0.0	
	C <sub>Ov</sub>	16.4	14.1	13.3	12.8	10.4	9.2	8.8	7.8	7.4	
	S <sub>Bz</sub>	80.0	77.9	78.8	79.1	84.0	83.7	84.1	84.5	86.2	
	Y <sub>Bz</sub>	29.1	23.7	23.0	22.3	20.4	18.0	17.3	15.5	15.4	
Ni/SBA-15	C <sub>Bz</sub>	73.5	69.0	67.8	66.8	66.4	66.3	65.8	65.6	65.2	1.0
	C <sub>Tu</sub>	53.0	44.8	43.5	41.2	40.1	39.4	38.3	37.7	36.7	
	C <sub>Xy</sub>	80.7	62.7	61.9	60.5	59.9	59.4	53.8	48.4	43.2	
	C <sub>Ov</sub>	94.1	93.7	91.8	89.2	87.9	87.1	82.7	78.7	74.6	
	S <sub>Bz</sub>	28.1	26.5	26.6	27.0	27.2	27.4	28.7	30.0	31.5	
	Y <sub>Bz</sub>	20.7	18.3	18.0	18.0	18.0	18.2	18.9	19.7	20.5	
Ni/MCM-41	C <sub>Bz</sub>	53.8	48.9	47.1	46.0	45.5	43.1	41.3	39.0	35.6	1.2
	C <sub>Tu</sub>	32.3	28.6	23.9	19.1	17.4	13.1	5.1	3.4	2.4	
	C <sub>Xy</sub>	0.0	0.0	0.0	0.0	2.6	4.9	5.0	5.4	5.6	
	C <sub>Ov</sub>	40.0	35.9	32.3	28.8	29.2	27.0	21.3	19.8	17.9	
	S <sub>Bz</sub>	48.4	49.0	52.5	57.6	56.1	57.4	69.7	71.2	71.5	
	Y <sub>Bz</sub>	26.1	24.0	24.7	26.5	25.6	24.7	28.8	27.8	25.5	

**Table 4.** Kinetics parameters and activation energies for hydrogenation reaction.

Temp. (°C)	Orders	Ni/HMS	Ni/MCM-41	Ni/SBA-15	Ni/FSM-16
		Power law model			
130	$n_{H_2}$	0.79	1.16	1.10	0.73
150	$n_{H_2}$	0.84	1.18	1.10	0.87
170	$n_{H_2}$	0.93	1.20	1.11	1.00
190	$n_{H_2}$	1.22	1.42	1.12	1.19
130	$m_{Bz}$	0.21	0.11	0.23	0.34
150	$m_{Bz}$	0.31	0.12	0.23	0.41
170	$m_{Bz}$	0.38	0.14	0.25	0.49
190	$m_{Bz}$	0.47	0.26	0.27	0.50
$E_{app}^{act}$ (kJ/mol)		81.18	83.51	41.95	92.30

		Langmuir-Hinshelwood model			
K	$E_{app}^{act}$ (kJ/mol)	80.60	86.1	69.37	98.05
	A (mol/g.s)	$2.7 \times 10^{-27}$	$1.0 \times 10^{-29}$	$3.0 \times 10^{-26}$	$2.5 \times 10^{-31}$
$K_{Bz}$	$-\Delta H_{ads-Bz}$ (kJ/mol)	3.59	3.59	3.59	3.59
	$A_{Bz}$ (atm <sup>-1</sup> )	$15.4 \times 10^2$	$15.4 \times 10^2$	$15.4 \times 10^2$	$15.4 \times 10^2$
$K_{H_2}$	$-\Delta H_{ads-H_2}$ (kJ/mol)	57.41	100.65	20.71	67.34
	$A_{H_2}$ (atm <sup>-1</sup> )	$41.1 \times 10^4$	131.0	$1.2 \times 10^{10}$	$68.1 \times 10^4$



**Fig. 4.** (a) Arrhenius plots, (b) double-log plots at a selected temperature (150 °C), estimated data by (c) power law model and (d) Langmuir-Hinshelwood model for Ni/SBA-15 catalyst at 150 °C

In this equation, n and m are the rate exponents of reaction:

$$r \left( \frac{\text{mol}}{\text{g.s}} \right) = k P_{H_2}^n P_{Bz}^m \quad (5)$$

k is the rate constant defined by Arrhenius equation;

$$k = A e^{-\frac{E_{app}^{act}}{RT}} \quad (6)$$

This equation gives the apparent activation energies ( $E_{app}^{act}$ ) and pre-exponential factors (A) reported in Table 4. The reaction rate was also calculated as follows:

$$r \left( \frac{\text{mol}}{\text{g.s}} \right) = \frac{\text{Bz flow rate} \times \text{Bz density} \times \text{conv.(\%)}}{\text{Bz molar weight} \times \text{weight of catalyst} \times \text{impregnated metal}} \quad (7)$$

The activation energies (42.95-92.30 kJ mol<sup>-1</sup>) obtained for benzene hydrogenation over the prepared catalysts (Table 4) are in a good agreement with similar reports of nickel catalysts in the benzene hydrogenation [26]. The Arrhenius plots for calculating these activation energies as a function of temperature are given on Fig. 4a. The relative reaction orders (Table 4) with respect to Bz and H<sub>2</sub> partial pressures (power-law fit shown in Fig. 4c) is symptomatic of stronger adsorption for hydrogen than benzene (positive exponents).

By the same token, Langmuir-Hinshelwood (LH) model [6] was also developed. The relevant key features of this model were provided on Table 4. The expression of this kinetics model, based on partial pressures of H<sub>2</sub> and Bz ( $P_{H_2}$  and  $P_{Bz}$ ) and rate constants of H<sub>2</sub> and Bz adsorptions ( $k_{H_2}$  and  $k_{Bz}$ ) can be expressed as follows:

$$r = \frac{k \cdot P_{Bz} \cdot P_{H_2}}{\left( \left( \frac{1}{k_{Bz}} \right) + P_{Bz} \right) \cdot \left( \left( \frac{1}{k_{H_2}} \right) + P_{H_2} \right)} \quad (8)$$

In this equation, the rate constant of adsorption is a Van't Hoff type equation:

$$k_x = A_x e^{-\frac{E_a^x}{RT}} \quad (9)$$

The estimated results with LH model achieve relatively the higher activation energies than the results measured with the PL model. Table 4 presents the pre-exponential factor of H<sub>2</sub> adsorption ( $A_{H_2}$ ) is higher than that of the Bz ( $A_{Bz}$ ). This probably implies a faster and stronger adsorption of H<sub>2</sub> over the prepared catalysts.

Figs. 4c & d show the comparison between the PL and LH models predictions and the experimental data for different catalysts. As it can be observed in these plots, the models predictions compare favorably with the obtained experimental data, indicating that the PL model has better correlation with the LH model.

However, this model is only a statistical model and does not consider any molecular interactions and their adsorptions.

#### 4. Conclusions

Gas-phase hydrogenation of benzene was tested at 130-190 °C and ambient pressure. This study successfully introduced nickel over the mesoporous supports. The structural and textural properties of these synthesized catalysts were measured using various analytical instruments. The XRD, FTIR and SEM analyses confirmed the formation of the desired structures and specific morphology for each catalyst. Subsequently, the N<sub>2</sub> and H<sub>2</sub>-sorption tests have greatly facilitated the justification of the performance of catalysts. The results obtained in this work clearly show that Ni catalyst containing SBA-15 has the best conversion of benzene, toluene and xylene with a good rate and reaction activation energy. This is despite the fact that the stability of this catalyst is very low due to the formation of coke and catalytic activity loss over time. On the other hand, this catalyst has very low selectivity to benzene in aromatics mixture. Combined with various characterizations analysis and catalytic tests, the better performance according to benzene selectivity and reaction yield was obtained from Ni/FSM-16. This result was attributed to the well improved textural properties, especially pore volume and width and their effects on selective performance.

#### References

- [1] X. Zhang, B. Gao, A. E. Creamer, C. Cao, Y. Li, J. Hazard. Mat. 338 (2017) 102-123.
- [2] T. Li, D. Xia, G. Zhou, H. Xie, Z. Jiao, X. Zhang, Catal. Commun. 112 (2018) 35-38.
- [3] K. Goundani, C. Papadopoulou, C. Kordulis, React. Kinet. Catal. Lett. 82 (2004) 149-155.
- [4] F. Dominguez, J. Sanchez, G. Arteaga, E. Choren, J. Mol. Catal. A: Chem. 228 (2005) 319-324.
- [5] X. Liu, S. Liu, P. Xu, Russ. J. Phys. Chem. A 91 (2017) 2098-2102.
- [6] M.H. Peyrovi, N. Parsafard, Z. Mohammadian, Chin. J. Chem. Eng. 26 (2018) 521-528.
- [7] L. Lozano, G.B. Marin, J.W. Thybaut, Ind. Eng. Chem. Res. 56 (2017) 12953-12962.
- [8] T. Bera, J.W. Thybaut, G.B. Marin, Ind. Eng. Chem. Res. 50 (2011) 12933-12945.
- [9] T. Bera, J.W. Thybaut, G.B. Marin, ACS Catal. 2 (2012) 1305-1318.
- [10] B. Mattson, W. Foster, J. Greimann, T. Hoette, N. Le, A. Mirich, S. Wankum, A. Cabri, C. Reichenbacher, E. Schwanke, J. Chem. Educ. 90 (2013) 613-619.
- [11] M.H. Peyrovi, N. Parsafard, M.A. Hajiabadi, Int. J. Chem. Kinet. 49 (2017) 283-292.

- [12] M.H. Peyrovi, M.R. Toosi, *React. Kinet. Catal. Let.* 94 (2008) 115-119.
- [13] M.H. Peyrovi, T. Rostamikia, N. Parsafard, *Energy Fuels* 32 (2018) 11432-11439.
- [14] Z. Mohammadian, M.H. Peyrovi, N. Parsafard, *ChemistrySelect* 3 (2018) 12639-12644.
- [15] Z. Mohammadian, M.H. Peyrovi, N. Parsafard, *Chem. Phys. Let.* 715 (2019) 367-374.
- [16] Y. Sun, C. Li, A. Zhang, *Appl. Catal. A* 22 (2016) 180-187.
- [17] V.V. Pushkarev, K. An, S. Alayoglu, S.K. Beaumont, G. A. Somorjai, *J. Catal.* 92 (2012) 64-72.
- [18] S. Akbayrak, *J. Colloid Interface Sci.* 530 (2018) 459-464.
- [19] T. Li, D. Xia, G. Zhou, H. Xie, Z. Jiao, X. Zhang, *Catal. Commun.* 112 (2018) 35-38.
- [20] R.A. Ortega-Domínguez, H. Vargas-Villagrán, C. Peñaloza-Orta, K. Saavedra-Rubio, X. Bokhimi, T.E. Klimova, *Fuel* 198 (2017) 110-122.
- [21] G. Ye, Y. Sun, X. Zhou, K. Zhu, J. Zhou, M.O. Coppens, *Chem. Eng. J.* 329 (2017) 56-65.
- [22] H. Xia, B. Liu, Q. Li, Z. Huang, A.S.C. Cheung, *Appl. Catal. B* 200 (2017) 552-565.
- [23] K.M.S. Khalil, *J. Colloid Interface Sci.* 315 (2007) 562-568.
- [24] L. Čapek, J. Adam, T. Grygar, R. Bulanek, L. Vradman, G. Košová-Kučerová, P. Čičmanec, P. Knotek, *Appl. Catal. A* 342 (2008) 99-106.
- [25] X. Shao, X. Zhang, W. Yu, Y. Wu, Y. Qin, Z. Sun, L. Song, *Appl. Surf. Sci.* 263 (2012) 1-7.
- [26] V. V. Pushkarev, K. An, S. Alayoglu, S. K. Beaumont, G. A. Somorjai, *J. Catal.* 292 (2012) 64-72.